Research Article ISSN: 2349-2678

Contents lists available at www.ijpba.in

International Journal of Pharmaceutical and Biological Science Archive

NLM (National Library of Medicine ID: 101738825)

Index Copernicus Value 2019: 71.05

Volume 11 Issue 4; July-August; 2023; Page No. 17-27

Non -Newtonian Fluid Flow over an Inclined Plate

Ch. Shivaprasad[1], Dr. Deepak Vats[2]

Research Scholar, Sunrise University, Alwar

Professor, Sunrise University, Alwar

Article Info: Received: 27-06-2023 / Revised: 08-07-2023 / Accepted: 12-08-2023

Address for Correspondence: Ch. Shivaprasad

Conflict of interest statement: No conflict of interest

Abstract

In this study, we explore the influence of radiation and surface temperature variation on the convective heat transfer of a nanofluid across an inclined plate. Nanoparticle-containing fluids other than water were also explored, including silver, aluminium oxide, and copper. Crank Nicolson, an effective tridiagonal iterative implicit finite difference approach, is used to acquire the solutions. Graphs and tables are used to examine and display the findings for a number of different factors. The findings are in remarkable accord with prior research. An inclined permeable stretching sheet is used to study the momentum, heat, and mass transfer behaviour of an MHD nanofluid flow containing conducting dust particles in the presence of radiation, a nonuniform heat source/sink, a volume fraction of nano particles, a volume fraction of dust particles, and a chemical reaction. We have proposed incorporating conductive dust particles into a Cu-water nanofluid. In order to numerically solve the governing partial differential equations of the flow, heat, and mass transfer, a similarity transformation is used to convert them into nonlinear ordinary differential equations. Using graphs, we illustrate how changes in a few non-dimensional controlling factors may alter the resulting velocity, temperature, and concentration profiles.

Keywords: MHD; Dusty fluid; Nanofluid; Chemical Reaction; Volume fraction; non-uniform heat source/sink

Introduction

The major benefit of nanofluid, a term coined and referring to a fluid based on smart nanotechnology that comprises a suspension of submicronic nano-scale particles, is that it improves the thermal conductivity of the base fluid, as seen. Because traditional fluids like water, ethylene, and mineral oils have such a low thermal conductivity compared with nanofluids, many recent publications have sought to better understand how nanofluids behave in contexts as diverse as industrial and engineering systems, nuclear reactors, electronics, and even advanced nuclear systems and medicine. described the existing and prospective uses of nanofluids in a variety of applications. used a mixed explicit implicit finite difference approach to solve a version of Rayleigh's issue that included an endless horizontal fluid through which a viscous incompressible fluid flowed after being impulsively initiated. investigated the major contribution for fluid dynamics after stokes. The issue of stokes for the vertical plate due to MHD was of concern. To further investigate natural convection on an isothermal flat plate, later used the implicit finite difference approach. The heat transfer in horizontal, vertical, and inclined plates with variable wall temperature and heat flow was studied, and a significant result was provided.

The effects of radiation on an unsteady magneto hydrodynamic free convection flow across a semi-infinite vertical porous plate subject to a transverse uniform magnetic field. In their next work, included a chemical reaction into their analysis of free convective viscous dissipative

radiative fluid flow across a vertically moving plate. investigated free convective flow through discrete parts of an inclined plate subject to magnetohydromagnetic action with non-uniform wall temperature. The findings for the nanofluid through a vertical plate were investigated Recently, MHD effects on the nanofluid past an inclined plate were investigated.

Literature Review

Z. Z. Rashed (2019) The effects of a uniform magnetic field and solar radiation on the free convective flow and heat transfer of a nanofluid near an inclined plate in a porous media have been investigated. The governing equations that allow for convective-radiative heat exchange with an environment have been formulated using the boundary-layer technique, the Boussinesq approximation, and the two-phase nanofluid model. The phenomena under consideration has been analyzed using the local similarity technique. Numerical solutions to the resulting equations have been found with the help of the MATLAB program. Nusselt number, temperature, and volume fraction of nanoparticles, as well as their profiles, have all been analyzed to see how control variables affect them.

Hang Xu (2022) We investigate the mixed convection flow of a hybrid nanofluid in an inclined channel under continuous heat flux and top wall-slip owing to wall stripe circumstances. Non-dimensional representations of the flow velocity, temperature, and pressure are provided with their corresponding explicit analytical solutions. The domain of the flow regime, the distributions of velocities and temperatures, and the influence of different physical factors including the volume fractions of hybrid nanoparticles, the wall-slip, the Grashof number, the Reynolds number, and the inclined angle are all examined and evaluated. It is discovered that both the wall-slip and the hybrid nanofluid put off the onset of flow reversal on the upper wall.

Raghunath Kodi (2021) The goal of this research is to simulate Soret-aligned magnetic field and chemical reaction as an unsteady hydrodynamic flow across an inclined plate embedded in a porous material. The diffusion equation is used to mix equal amounts of momentum, energy, and mass to create the dimensionless momentum/energy/mass model. The behavior of the fluid's velocity, temperature, and concentration on the slanted vertical plate was analyzed computationally by changing the alignment of the magnetic field, the Casson parameter, the inclination angle, the kind of chemical reaction, and the soret parameter. The tables for the various parameters contain the results obtained from the skin friction, Nusselt number, and Sherwood number. The findings are consistent with a subset of previously reported research. The current study reports that a slowing impact on velocity is maintained by the existence of an inclination angle, a magnetic field that is aligned with the direction of motion, and the Casson fluid parameters. As the inclination angle, magnetic field alignment parameter, and Casson fluid parameter are all increased, the velocity drops. The findings compare well to similar work that has been published elsewhere.

N. Sandeep (2016) This paper deals with the momentum, heat and mass transfer behaviour of MHD nanofluid flow embedded with conducting dust particles past an inclined permeable stretching sheet in presence of radiation, nonuniform heat source/sink, volume fraction of nano particles, volume fraction of dust particles and chemical reaction. We have considered Cu-water nanofluid embedding with conducting dust particles. The governing partial differential equations of the flow, heat and mass transfer are transformed into nonlinear ordinary differential equations by using similarity transformation and solved numerically using Runge-Kuttabased shooting technique. The effects of non-dimensional governing parameters on velocity, temperature and concentration profiles are discussed with the support of graphs. Also, skin friction coefficient, Nusselt and Sherwood numbers are discussed and presented through tables. Under some special conditions present results have good agreement with the existed results. It is observed a raise in the heat transfer rate due to increase in the fluid particle interaction parameter. It is also observed that an increase in

chemical reaction parameter enhances the mass transfer rate of the dusty nanofluid.

M. Ferdows (2014) A numerical study of the boundary layer flow past unsteady stretching surface in nanofluid under the effects of suction and viscous dissipation is investigated. The model used for the nanofluid incorporates the effects of Brownian motion and thermophoresis. A similarity solution is presented, which depends on the unsteadiness parameter A, Eckert number Ec, ζ suction or injection parameter, Prandtl number Pr, Lewis number Le, Brownian motion number Nb, and thermophoresis number Nt. The governing partial differential equations were converted to nonlinear ordinary differential equations by using a suitable similarity transformation, which are solved numerically using the Nactsheim-Swigert shooting technique together with Runge-Kutta six-order iteration scheme. The accuracy of the numerical method is tested by performing various comparisons with the previously published work, and the results are found to be in excellent agreement.

Methodology

Each absorber plate was 1800 mm long by 900 mm wide by 1 mm thick. In all scenarios, 40 mm was kept as the space between the glazing and absorber plate and the bottom and absorber plate. The diameter of the perforations in the perforated plate was 1.5 mm, and the distance between adjacent holes was 10 mm. depicts the shape of the perforated and solid mild steel absorber plates used in the solar air heater.

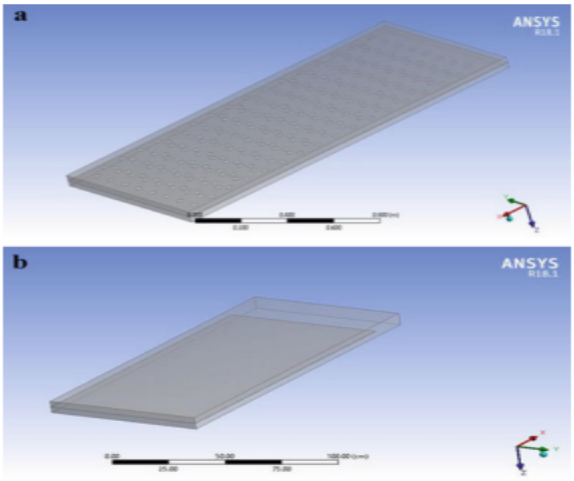

Figure 1: a) Perforated plate double pass. B) Flat plate double pass

Governing Mathematical Relationships

Below are the simulation assumptions made by ANSYS: FLUENT 18.1. Tabulated in Table 1 are the specifics of the boundary conditions.

i. It is assumed that the air flow serving as the working fluid is incompressible.

ii. Working fluid maintains its temperature and physical qualities at all times.

The heat transfer analysis shows consistent airflow and no wall slide.Below are provided [24] the general mathematical equations of continuity, motion, and energy**:**

$$\frac{\partial}{\partial x_i}(\rho v_i) = 0 \quad (1)$$

$$\frac{\partial}{\partial x_j}(\rho v_i v_j) = \left[-\frac{\partial p}{\partial x_i} + \frac{\partial}{\partial x_j}\left[\mu\left(\frac{\partial v_i}{\partial x_j} + \frac{\partial v_j}{\partial x_i}\right)\right] - \frac{2}{3}\mu\frac{\partial v_k}{\partial x_k}\partial_{ij}\right] \quad (2)$$

$$\frac{\partial}{\partial x_j}\left(\rho v_j C_p T - k\frac{\partial T}{\partial x_j}\right) = u_j\frac{\partial p}{\partial x_j} + \mu\left(\left(\frac{\partial v_i}{\partial x_j} + \frac{\partial v_j}{\partial v_i}\right) - \frac{2}{3}\frac{\partial v_k}{\partial x_k}\partial_{ij}\right) \quad (3)$$

Research on solar air heater efficiency using the k-E model. The restrictions placed on the duct's perforated and flat plates by the boundary conditions. A turbulent and incompressible local flow was assumed. Inlet and outflow

boundary conditions for velocity and pressure were set.

the controlling mathematical connection is as follows:

$$\frac{\partial}{\partial x_i}(\rho k v_i) = \frac{\partial}{\partial x_j}\left[\left(\frac{\mu+\mu_t}{\sigma_k}\right)\frac{\partial k}{\partial x_j}\right] + \mu_t\left[\frac{\partial v_i}{\partial x_j} + \frac{\partial v_j}{\partial v_i}\right]\frac{\partial v_i}{\partial x_j} - \rho\varepsilon \quad (4)$$

$$\frac{\partial}{\partial x_i}(\rho\varepsilon v_i) = \frac{\partial}{\partial x_j}\left[\left(\frac{\mu+\mu_t}{\sigma_\varepsilon}\right)\frac{\partial \varepsilon}{\partial x_j}\right] + C_{1\varepsilon}\frac{\varepsilon}{k}\mu_t\left[\frac{\partial v_i}{\partial v_j} + \frac{\partial v_j}{\partial v_i}\right]\frac{\partial v_i}{\partial v_j} - C_{2\varepsilon}\rho\frac{\varepsilon^2}{k} - \alpha\rho\frac{\varepsilon^2}{k} \quad (5)$$

Viscosity modeling in turbulence:

Table 1: Boundary condition for computation of perforated duct solar air heater.

Boundary region	Type of region	flow rate (kg/s)	Pressure (Pa)	Temp. (K)
Inlet	Velocity	0.08	101,315	298
Outlet	Pressure	Out flow	101,305	340
Duct wall	Wall	No slip	–	–
Absorber	Wall	No slip	–	370

Table 2: Grid independency test

Refining levels	Number of elements	Percentage variation of air temperature	Percentage variation pressure drop
1	120,000	3.9	4.9
2	180,000	2.5	3.0
3	320,000	0.54	0.60
4	360,000	0.40	0.55

$$\mu_t = \rho C_\mu \frac{k^2}{\varepsilon}$$

Experimental studies of basic turbulent and shear flows, such as boundary, mixing layer, and jet flows, or decaying isotropic grid turbulence, have yielded the stated constants. For a wide enough variety of shear flows, both confined and unconfined, it works just well.

Grid Convergence Test

By continuously decreasing cell size, grid convergence tests quantify how much better computing outputs are. As the mesh size is reduced, it should approach the true values. Common CFD procedure involves using a large initial mesh size and iteratively refining it until the apparent variations in the results fall below an acceptable error threshold (Table 2). The domain for a 2D channel with these dimensions was evaluated for use in the perforated duct analysis: 1800 mm in length, 900 mm in width, and 40 mm in channel height. Four distinct meshes were validated to describe the necessary number of elements. As can be seen in Table 2, admitting different grid pieces helped pass the grid independence test. Tests of grid independence indicate that 320,000-element grids guarantee a good result. After 320k, there is obviously no longer a significant percentage difference in valuation metrics.

Data Reduction

Reynolds, Nusselt numbers, average heat transfer coefficient, hydraulic diameter and pressure drop in the perforated and flat plate ducts are given by Eqs. (7)–(11).

$$R_e = \frac{\rho V D_h}{\mu}$$

$$\overline{Nu} = \frac{\bar{h} D_h}{k}$$

$$\bar{h} = \frac{Q_w}{A_{duct}(\overline{T}_{wall} - \overline{T}_{fluid})}$$

$$D_h = \frac{4A}{P}$$

$$\Delta P_{duct} = \frac{\rho V^2 4 f L}{2 D_h}$$

Results and Discussion

Using a Runge-Kutta based shooting approach, we numerically solve the linked ordinary differential Eqs. (15) to (21) under the boundary conditions (22). The obtained results demonstrate the effect of the non-dimensional governing parameters on the velocity, temperature, and concentration profiles for the fluid and dust phases, specifically the volume fraction of nano particles, the mass concentration of the dust particles, the fluid particle interaction parameter for velocity, the non-uniform heat source/sink parameter * A, and the chemical reaction parameter K r. We used * * 2, 1, 0.1, M R A B for our numerical findings. Ec d = 0.8, 0.4,Pr 6.2, /3, 0.6, 0.2, T Sc Kr = 0.5, Gc K = 1.0, and Pr = 6.2. Except for the different numbers given in the various figures and tables, they are held constant throughout the whole research.The thermophysical characteristics of water and copper are shown in Table 3.

Table 3: Thermophysical properties of water and Cu nano particles.

	ρ (Kgm^{-3})	c_p $(Kg^{-1}K^{-1})$	k $(Wm^{-1}K^{-1})$	β $(10^{-5}K^{-1})$
H_2O	997.1	4179	0.613	21
Cu	8933	385	401	1.67

Figures 3-4 show how the volume percentage of nanoparticles affects the flow's velocity, temperature, and concentration. Clearly, the flow's velocity, temperature, and concentration profiles all benefit from a higher volume percent of nanoparticles, while the concentration profiles suffer. This is because an increase in the nanoparticle volume fraction increases the thermal boundary layer thickness and the velocity. Particles migrate away from the surface (or their phase shifts to cooler places) as a result of this thickening of the thermal boundary layer. Because of this, the concentration profiles of the flow have been decreasing.

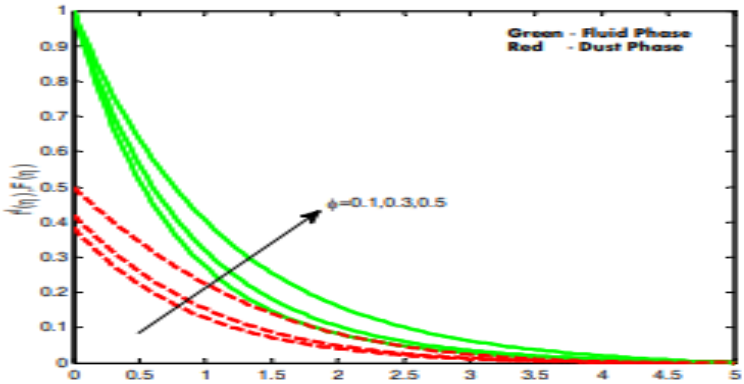

Figure 2: The velocity distributions of nanoparticles with varying volume fractions.

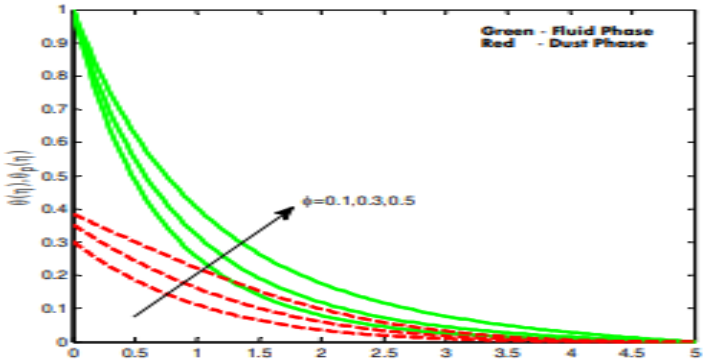

Figure 3: Changes in temperature as a function of nanoparticle volume %.

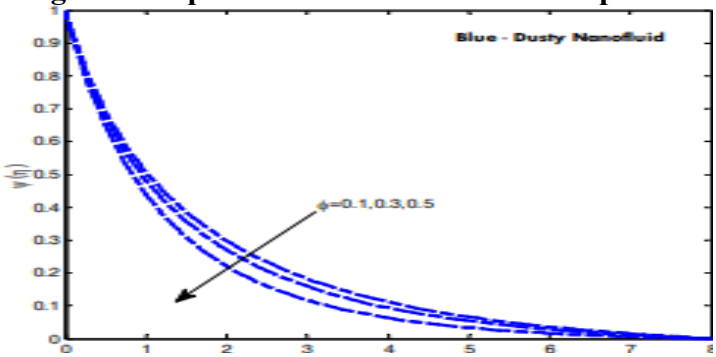

Figure 4: Nanoparticle concentration profiles over a wide range of volume fraction values.

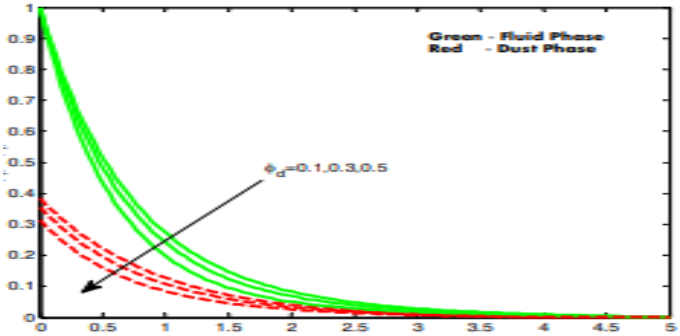

Figure 5: Dust particle velocity distributions over a range of volume fractions.

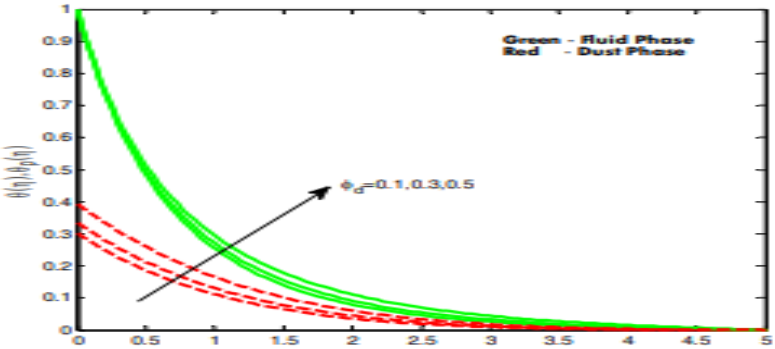

Figure 6: Temperature distributions for different dust volume fractions.

Depict the changes in flow velocity, temperature, and concentration as a function of dust particle volume percent. The concentration profiles of the flow are decreased while the velocity and temperature profiles of the fluid and dust phases are raised in response to an increase in the volume fraction of dust particles. However, we found a large discrepancy in how the dust phase's velocity and temperature profiles evolved in the region close to the wall. and 2 show that the dust phase's velocity and temperature profiles peak in close proximity to the plate. show that, unlike the situation with a volume proportion of dust particles, the maximum values achieved by the velocity and temperature profiles are smaller. Moreover, the

free stream velocities are reached by the velocity profiles at the 3 level, as shown in. In contrast, at 2.5, the free stream velocity was attained in velocity profiles. The results show that the momentum and thermal boundary layer thickness are significantly increased by an increase in the volume fraction of nano particles compared to an increase in the volume fraction of dust particles.

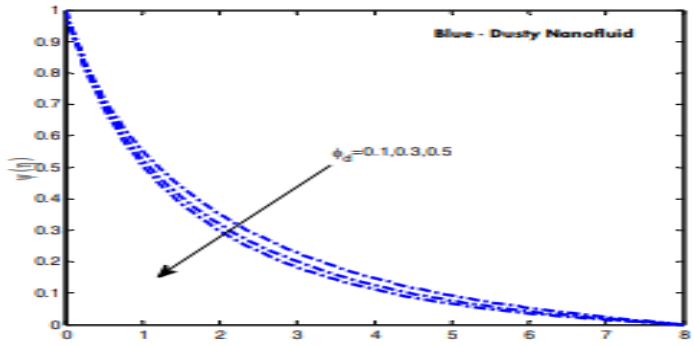

Figure 7: Concentration profiles at different dust particle volume fractions.

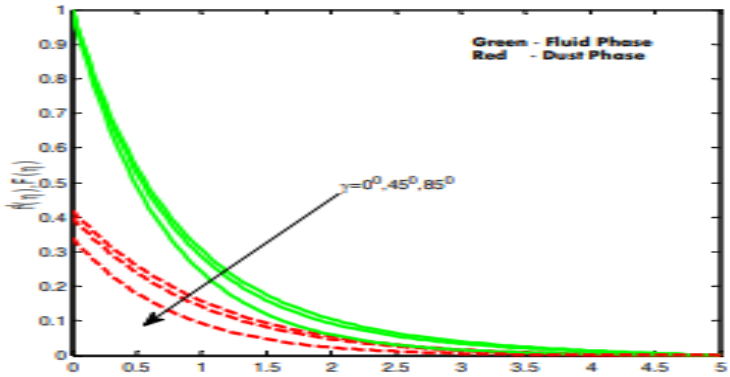

Figure 8: Various velocity distributions as a function of angle of tilt.

Show how the flow's velocity, temperature, and concentration profiles change depending on the angle of the inlet. A decrease in the velocity field and an increase in the temperature and concentration field have been seen when the angle of inclination rises. This is because the largest gravitational force exerts on the flow when the sheet is in the vertical direction, at 0. Because buoyancy forces weaken as the sheet becomes more horizontal, the velocity boundary layer thins while the thermal boundary layer thickens. Concentration profile flows were found to be improved as a result of buoyancy force variations**.**

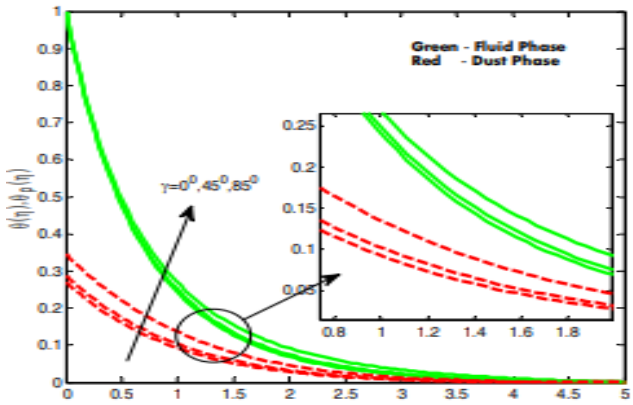

Figure 9: Temperature distributions at different angles of inclines.

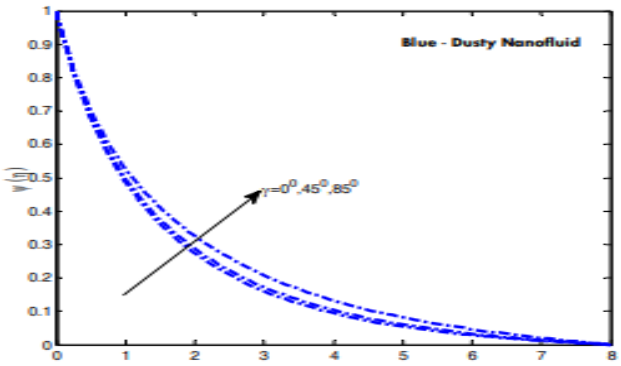

Figure 10: Profiles of concentration over a wide range of slant angles.

The influence of the radiation parameter on the flow temperature profiles. Clearly, improving the temperature profiles of the fluid and particle phase requires increasing the value of the radiation parameter. An increase in the radiation parameter often allows the heat energy to be transferred to the flow. The thickness of the thermal boundary layer rises as a result of this. This suggests that the effect of radiation is larger if R is less than zero and negligible if R is more than. This is consistent with the radiation parameter's typical physical behavior. the fluid and dust phase temperature curves as a function of dust particle mass concentration. The temperature fields of the fluid and dust phases are shown to degrade with an increase in the mass concentration of the dust particles.

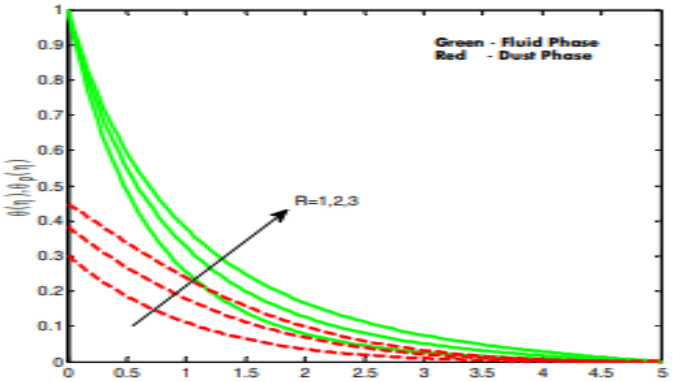

Figure 11: Comparison of temperature distributions for different values of the radiation parameter.

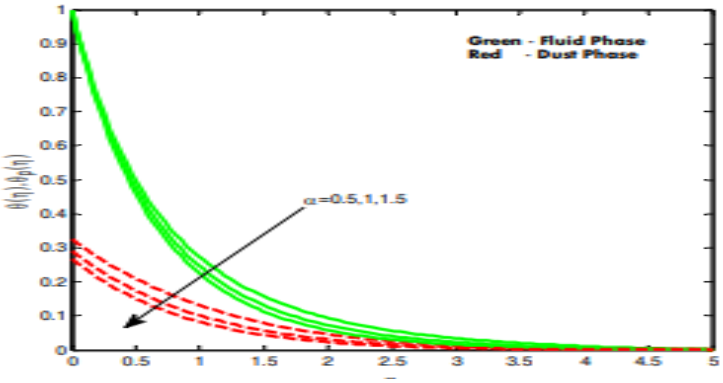

Figure 12: Dust concentration-temperature profiles for a range of values.

Temperature distributions in the fluid and dust phases are shown to be affected by the fluid particle interaction parameter for temperature () T, as shown in. We found it fascinating that when we increased the value of T, the dust phase temperature profiles improved while the fluid phase temperature profiles deteriorated. This is because an increase in the thermal

conductivity of the flow causes a rise in the fluid particle interaction parameter. Because of this, the fluid phase temperature profiles dropped and the heat transfer rate rose. Concentration profiles in the flow as a function of the chemical reaction parameter are. It is evident that the concentration profiles are depreciated and the mass transfer rate of the dusty nanofluid is increased when the chemical reaction parameter is raised.

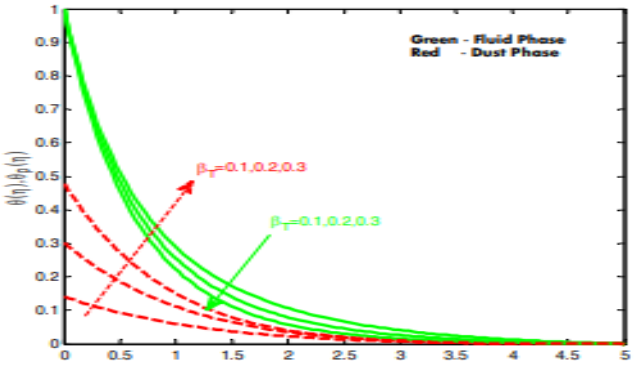

Figure 13: Temp profiles for different values of the parameter that determines how hot or cold fluid particles interact.

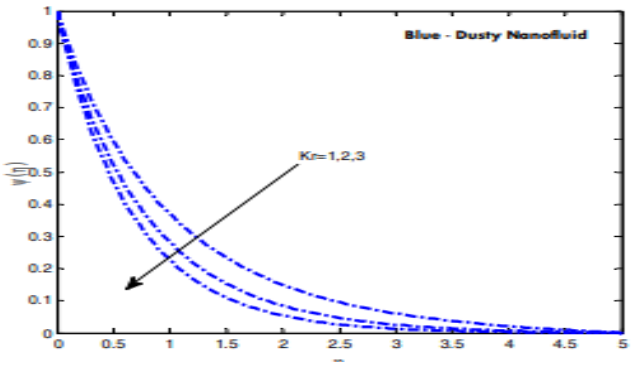

Figure 14: Chemical reaction concentration profiles for a range of parameters.

The influence of non-uniform heat source/sink characteristics on the fluid and dust phase temperature the temperature distributions of the fluid and dust phases are found to be improved by increasing the values of * A and * B. It's easy to deduce that when * A and * B are both positive, they function as heat producers, whereas when they're both negative, they function as heat watchers. In most cases, heat energy is released into the flow when it is generated. Because of this, the flow's temperature profiles are improved. Therefore, both * A and * B conform to the physical law of the same heat source parameter**.**

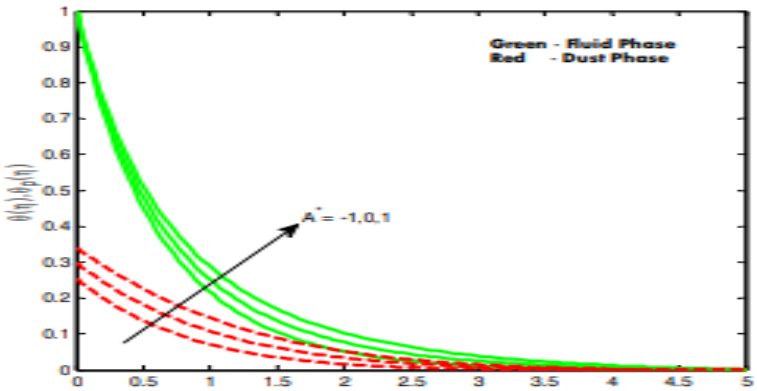

Figure 15: Temperature profiles for various values of non-uniform heat source/sink

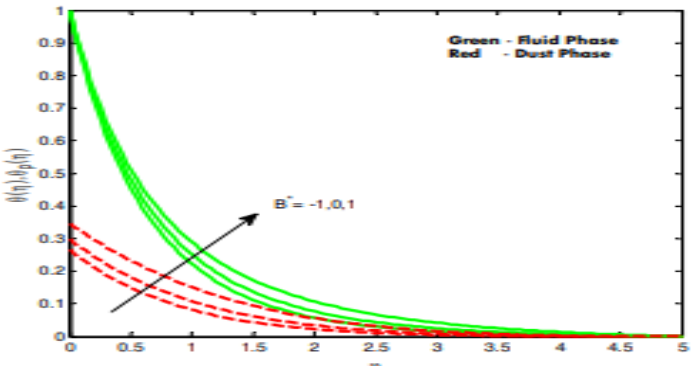

Figure 16: Temperature profiles for various values of non-uniform heat source/sink.

In Table 2, we can see how our current findings compare. Present findings exhibit a great agreement with the existing results under certain particular situations. This demonstrates the reliability of the current conclusions and the numerical method we used in this investigation. The friction factor, Nusselt, and Sherwood numbers are shown to be affected by the nondimensional controlling factors in Table 3.

According to the data in the table, the skin friction coefficient, heat transfer rate, and dust particle volume percent all decrease as the inclination angle and dust particle volume fraction increase. An increase in slant lessens the impact of buoyant forces on the current. As a result, heat and mass transport are slowed down considerably.The friction factor, Sherwood number, and heat transfer rate all improve with an increase in dust particle mass concentration and the temperature of the fluid interacting with the dust particles. Because the flow's thermal conductivity is growing, this happens. The skin friction coefficient, the mass transfer rate, and the Nusselt number all improve with higher values for the radiation parameter, the non-uniform heat source/sink parameter, and the chemical reaction parameter. Friction close to the wall is created physically when external heat is generated. The level of friction has increased for this reason.The friction coefficient is decreased, and the rate at which heat and mass may be transferred is increased, as the volume percentage of nano particles increases. The contact between the fluid phase and the nanoparticle phase is enhanced as the volume fraction of nanoparticles increases, leading to a higher rate of heat and mass transfer.

Conclusion

Both a flat-plate and a double-pass perforated solar air heater (SAH) have been subjected to CFD study using Ansys FLUENT 18.1. Each absorber plate was 1800 mm long by 900 mm wide by 1 mm thick. The governing equations are discretized using the finite volume technique (FVM). Computational studies reveal that, for a given mass flow rate of air of 0.08 kg/s, a perforated plate double pass is much more thermally efficient than a flat plate one.Average pressure drop at outflow for perforated plate SAH was 0.20 Pa; lowest air temperature 325 K; maximum air temperature 335 K; for average sun radiation 750 W/m2.

References

1. Rashed, Z. & Ahmed, Sameh & Sheremet, Mikhail. (2019). MHD Buoyancy Flow of Nanofluids Over an Inclined Plate Immersed in Uniform Porous Medium in the Presence of Solar Radiation. Journal of Mechanics. 35. 1-14. 10.1017/jmech.2018.40.
2. Xu, H. Mixed convective flow of a hybrid nanofluid between two parallel inclined plates under wall-slip condition. Appl. Math. Mech.-Engl. Ed. 43, 113–126 (2022). https://doi.org/10.1007/s10483-021-2801-6
3. Raghunath Kodi (2021) Unsteady MHD oscillatory Casson fluid flow past an inclined vertical porous plate in the presence of chemical reaction with heat absorption and Soret effects Volume 51, Issue 1 Pages: 1-1252 January 2022. https://doi.org/10.1002/htj.22327
4. N. Sandeep (2016) Heat and Mass Transfer in Nanofluid Flow over an

Inclined Stretching Sheet with Volume Fraction of Dust and Nanoparticles Journal of Applied Fluid Mechanics, Vol. 9, No. 5, pp. 2205-2215, 2016. Available online at www.jafmonline.net, ISSN 1735-3572, EISSN 1735-3645

5. Ferdows, M. S., S. M. Chapal and A. A. Afify (2014). Boundary layer flow and heat transfer of a nanofluid over a permeable unsteady stretching sheet with viscous dissipation. J. Eng. Thermophysics 23(3), 216-228.
6. Wong KV, De Leon O. 2010. Applications of nanofluids: current and future. Advances in Mechanical Engineering. 2:519659
7. Stokes GG. 1851 Jan. On the effect of the internal friction of fluids on the motion of pendulums. Cambridge: Pitt Press
8. Chen TS, Tien HC, Armaly BF. 1986. Natural convection on horizontal, inclined, and vertical plates with variable surface temperature or heat flux. International journal of heat and mass transfer. 29:1465-78
9. Selva rani M and Govindarajan A 2017 MHD Effects on Natural Convective Flow Of A Nanofluid Past An Inclined Plate With Heat Generation/Absorption Proc., Fourth int.,l conf., on Nanoscienes and Nanofluids (ICONN - 2017), 9-11 August 2017, SRM University, Kattankulathur, India
10. Kuznetsov AV, Nield DA. 2010. Natural convective boundary-layer flow of a nanofluid past a vertical plate. International Journal of Thermal Sciences. 49(2):243-7
11. Vajravelu, K., K. V. Prasad, J. Lee, C. Lee, I. Pop and R. A. V. Gorder (2011). Convective heat transfer in the flow of viscous Ag-water and Cu-water nanofluids over a stretching surface.Int.J.Thermal Sciences, 50(5), 843- 851.
12. Singh, A. K. and N.P.Singh (1996). MHD flow of a dusty visco-elastic liquid through a porous medium between two inclined parallel plates.Proceeding of national academy of science India 29(2), 143-150.
13. Rohni, A. M., S.Ahmad and I.Pop (2014). Flow and heat transfer at a stagnation point over an exponentially shrinking vertical sheet with suction. Int J Thermal Sciences 75, 164-170.
14. Sandeep, N. and V. Sugunamma (2014). Radiation and inclined magnetic field effects on unsteady MHD convective flow past an impulsively moving vertical plate in a porous medium. Journal of Applied Fluid Mechanics 7(2), 275-286
15. Hassan, H. (2014). Heat transfer of Cu-water nanofluid in an enclosure with a heat sink and discrete heat source.European J. Mechanics B/Fluids 45, 72-83.